Transport Properties of Bi_2Te_3†

H. A. Ashworth* and J. A. Rayne
Carnegie-Mellon University, Pittsburgh, Pennsylvania 15213

and

R. W. Ure, Jr.
University of Utah, Salt Lake City, Utah 84112
(Received 19 October 1970)

Measurements of the low-field magnetoresistance coefficients for both n- and p-type Bi_2Te_3 have been made at 77 and 4.2 K as a function of carrier concentration. Results for samples with low carrier densities are satisfactorily interpreted in terms of a previously proposed multiellipsoidal model of the valence- and conduction-band minima. Comparison of the observed galvanomagnetic coefficients with those predicted from de Haas–van Alphen (dHvA) experiments indicates that the relaxation time is anisotropic for both holes and electrons. Formulas which allow for anisotropic scattering are presented and the results combined with dHvA data to determine the relaxation-time tensor as a function of carrier concentration. For n-type samples with a carrier density greater than $4\times10^{18}\,\mathrm{cm}^{-3}$, the observed behavior is explained in terms of a simple two-band model and the anisotropy of the second band is shown to be relatively small. The presence of the second band appears to affect the scattering rates for the lower conduction band. A similar analysis is carried out for p-type Bi_2Te_3, but the results are less satisfactory.

I. INTRODUCTION

Measurements of the electrical transport properties in single crystals of metals and semiconductors have long been an established technique for acquiring information about their electronic structure. The first attempts to deduce the band structure of Bi_2Te_3 were based on magnetoresistance studies made several years ago by Drabble and his co-workers.[1–3] More recently, the electronic structure of n-type Bi_2Te_3 has been studied using the de Haas–van Alphen (dHvA) technique[4] and specific-heat measurements.[5]

The present study extends previous magnetoresistance measurements on n-type Bi_2Te_3, over a wide range of carrier concentrations, to liquid-helium temperatures. The results thus obtained are shown to be consistent with a six-ellipsoid model of the conduction-band minima similar to the model originally proposed by Drabble. However, the data indicate that two effects seriously distort the results of any simple theory of the transport properties. The first effect, originally proposed as a result of resistivity measurements[6–8] and subsequently as a result of the dHvA studies,[4] concerns the existence of the second conduction-band minimum which strongly influences the transport properties of all samples with carrier concentrations above $5\times10^{18}\,\mathrm{cm}^{-3}$. The second factor which must be considered is the presence in Bi_2Te_3 of an anisotropic scattering mechanism for electrons.

The present work is primarily concerned with the correct interpretation of the transport properties, using the six-ellipsoid model originally proposed, but taking into account the two effects mentioned above. In addition, by combining the results of the transport measurements with other independent determinations of the band parameters, it is possible to present a detailed evaluation of the anisotropy of electron scattering for both impurities and phonons.

Magnetoresistance measurements on p-type Bi_2Te_3 have previously been made by Drabble[2] and Efimova *et al.*[9] These data have been interpreted in terms of a six-valley ellipsoidal model for the valence band, which is also consistent with the results of high-field dHvA experiments.[10] However, more recent work[11,12] has indicated evidence for the existence of a set of valence-band maxima. Consequently, several p-type samples have also been measured to examine the possible effects of this more complicated band structure on the transport properties.

II. ELECTRONIC STRUCTURE OF Bi_2Te_3

A. General Properties of Bi_2Te_3

Bi_2Te_3 has a rhombohedral unit cell (space group $R\bar{3}m$) and is distinguished by a high degree of anisotropy in most of its physical properties. The c/a ratio is equal to 6.95, and results in the Brillouin zone illustrated schematically in Fig. 1. This figure shows the principal symmetry elements, which consist of a threefold axis in the trigonal direction $0z$, a twofold axis along the binary direction $0x$, and a mirror plane perpendicular to the binary axis containing the bisectrix direction $0y$. The remaining equivalent binary and bisectrix axes are related to

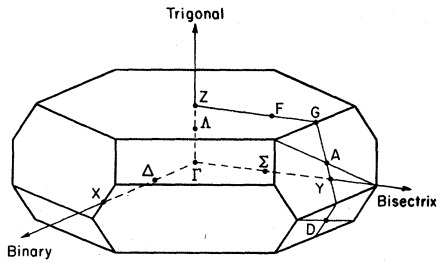

FIG. 1. Brillouin zone for Bi_2Te_3 showing principal symmetry points.

those shown by rotations of 120° and 240° about the trigonal axis. It is important to define the relation between the Brillouin zone and the positive sense of the trigonal and bisectrix directions to determine uniquely the energy-band parameters and magnetoresistance coefficients. The choice made in Fig. 1 is the most common one, and corresponds to the positive bisectrix direction lying along the projection of a rhombohedral vector. Earlier papers[3] on Bi_2Te_3 have made the choice that directs the bisectrix direction 180° away from the rhombohedral projection. In the following, it will be convenient to designate the binary, bisectrix, and trigonal directions by the indices 1, 2, and 3, respectively.

B. Conduction-Band Structure

The most precise determination of the conduction-band structure has been made by the dHvA technique.[4] The dHvA data have been satisfactorily interpreted for samples with carrier concentrations of less than 5×10^{18} cm^{-3} by assuming that the energy of a carrier can be expanded in the vicinity of the minimum in the usual quadratic form

$$E = (\hbar^2/2m)\,\alpha_{ij}k_ik_j\ . \qquad (1)$$

In this equation, α_{ij} is the inverse effective-mass tensor, k_i is the wave vector referred to the crystal axes at the local minimum for a representative valley, and repeated indexes are summed. In particular, it is found that the dHvA measurements, as well as the earlier magnetoresistance data, can be explained by a multivalley conduction band consisting of a set of six equivalent ellipsoids lying in mirror planes. For this case, the nonzero elements of the inverse effective-mass tensor reduce to α_{11}, α_{22}, α_{33}, and α_{23}; the other elements being zero from symmetry arguments. Table I summarizes the results of the measurements.

The dHvA data also indicate the existence of a second conduction band lying 30 meV above the first. The presence of this second band has been deduced by comparing the number of carriers determined from the Hall effect n_H with the number of carriers contributing to the dHvA effect n_E. While the two densities agree for samples with n_H less than 5×10^{18} cm^{-3}, it is found that n_H is greater than n_E above that concentration. This discrepancy indicates that some carriers are not contributing to the dHvA effect, presumably due to the existence of a second low-mobility band which begins to fill at a carrier concentration of about 5×10^{18} cm^{-3}, or at a Fermi energy of approximately 30 meV. Table I shows that, despite the presence of this second band, the inverse effective-mass tensor is virtually unchanged over the range of carrier concentrations studied.

There have been several attempts at calculating the band structure of Bi_2Te_3,[13–15] but as yet the agreement between experiment and these calculations is not satisfactory. The source of the disagreement stems partly from the heavy mass of Bi and Te, which can be expected to cause large spin-orbit coupling effects. In fact, the band gap (about 0.15 eV) is of the same size as estimates of the spin-orbit correction to the energy levels, which cannot be calculated with any accuracy. In spite of these difficulties, the pseudopotential calculation of Borghese and Donato[14] yields a six-valley model for both the valence and conduction bands, with the band edges along ΓD. The gap is indirect, and the nearest band edges for both valence and conduction band appear to be located at Γ.

C. Valence-Band Structure

As can be seen from Table I, the band parameters for p-type Bi_2Te_3 determined from dHvA measurements[10] show a remarkable similarity to those of the n-type material. From simultaneous Hall measurements in fields up to 150 kG, it has been concluded that there are six-hole ellipsoids. The agreement between the dHvA parameters and those determined from galvanomagnetic measurements at 77 K is fairly good. Magnetoresistance measurements have been extended to 4.2 K by Efimova *et al.*[9]; the parameters for the anisotropic scattering have been deduced, with the possibility of a second valence band being rejected.

More recent measurements of the high-temperature thermal conductivity[11] have indicated evidence

TABLE I. Components of the inverse effective-mass tensor and the thermal effective mass determined from dHvA experiments.

Author	α_{11}	α_{22}	α_{33}	α_{23}	m^*/m[a]
Mallinson *et al.* (low n) (Ref. 4)	34.6	4.35	6.86	1.53	0.105
Mallinson *et al.* (high n) (Ref. 4)	35.1	4.27	7.13	1.83	0.105
Testardi *et al.* (p type) (Ref. 10)	20.8	2.80	4.65	−1.05	0.150

[a]Determined from $m^*=m[\,\alpha_{11}(\alpha_{22}\alpha_{33}-\alpha_{23}^2)\,]^{-1/3}$.

for a valence-band structure with a subsidiary maximum 20 meV below the first. In an experiment similar to that of Mallinson,[4] Parfen'ev[12] has apparently confirmed the existence of the second valence band. These results and the magnetoresistance data are contradictory, since all the experiments have been carried out on samples with a carrier density greater than 10^{19} cm^{-3} and the effects of the second band should be noticeable in every case. Consequently, the information regarding valence-band structure must be regarded as somewhat in doubt. The most likely picture is a six-valley ellipsoidal model, probably with a subsidiary maximum 20 meV below the first.

III. EXPERIMENTS

A. Samples

The samples used in these experiments were spark cut from Bi_2Te_3 ingots grown by a horizontal loaded-zone technique from 99.999% pure starting materials. The approximate dimensions of a typical sample are 13 mm long and 2 mm on a side. Samples grown from a stoichiometric melt are p type with a hole concentration of about 2×10^{19} cm^{-3}. By adding excess tellurium or a dopant such as iodine to the melt, n-type samples are obtained. While iodine-doped samples are generally more homogeneous than those with tellurium doping, they also have a much lower mobility.[8] Consequently, the majority of the n-type samples studied were tellurium doped, although one iodine-doped sample was also studied in detail to examine the effects of different scattering centers (ionized tellurium and iodine atoms) on the transport properties, especially at helium temperatures, where ionized impurity scattering appears to be the dominant mechanism.

Measurements of semiconductors such as Bi_2Te_3 are often distorted by any of the following effects: inhomogeneity of the specimens, non-Ohmic contacts, surface effects, and geometrical effects. For all of the samples used in the present study, the homogeneity has been checked by comparing the carrier concentrations at various points on the sample and by requiring that the concentrations, thus determined, agree to within 10%. The current leads to the sample are made by first plating the ends of the samples with nickel and then soldering platinum wires to the plating. Voltage contacts are small beads of Pt-Rh wire applied to the middle of the sample by pressure only. Contacts made in this fashion remain Ohmic at all temperatures and currents (typically 0.5 A) used. The beads for the voltage contacts are small in diameter compared to the size of the sample and the contact separation is less than one-third the total length of the sample. The reproducibility of data taken for different contact separations and sizes indicates the absence of geometrical effects or current distortions.

Finally, the natural cleavage plane of Bi_2Te_3 provides a demonstration of the absence of surface effects. The samples used in this study are always cut such that the long direction of the sample (the current direction) is perpendicular to the trigonal axis. Samples grown perpendicular to the cleavage plane proved too mechanically weak to be measured. With the current flowing in a cleavage plane, data are always taken with voltage contacts on two distinctly different sets of surfaces. In one case, the voltage contacts are mounted on a surface that was spark cut and subsequently etched and in the second case the contacts rested on a "natural" surface that required no preparation other than a fresh cleave. The remarkable consistency between the data from the two different surfaces seems to be good indication that the measurements reported here reflect bulk properties and not surface effects.

B. Method

The purpose of the experiment is to determine the tensor coefficients in the familiar expansion of the resistivity in the presence of an external magnetic field[16]

$$E_i = \rho_{ij}J_j + \rho_{ijk}J_j B_k + \rho_{ijkl}J_j B_k B_l \ . \qquad (2)$$

Although there are 12 independent coefficients for a crystal of symmetry $R\bar{3}m$, the extreme mechanical weakness of Bi_2Te_3 samples cut parallel to the trigonal axis prevents measurements of ρ_{33}, ρ_{3333}, and ρ_{3311}. In addition, measurements of the off-diagonal elements ρ_{2311} and ρ_{2323} are seriously affected by contact misalignments and by the necessity to extract the relevant voltages from a large background due to the principal coefficients. Consequently, the present measurements have been restricted to

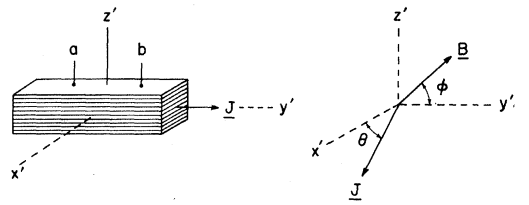

$\theta = 90°$, $\phi = 0°$, ρ_{2222}
$\theta = 90°$, $\phi = 90°$, ρ_{2233}

(a)

$\theta = 0°$, $\phi = 90°$, ρ_{2233}
$\theta = 0°$, $\phi = 0°$, ρ_{2211}

(b)

FIG. 2. Schematic diagram showing method of rotating the sample and magnetic field to obtain the magnetoresistance coefficients. The current direction is parallel to the cleavage planes, while the potential contacts are assumed to be on the cleavage surface. The planes of rotation for the field and current are $0y'z'$ and $0x'y'$, respectively, where $0z'$ is parallel to the trigonal axis of the crystal.

TABLE II. Measured values of the magnetoresistance coefficients at 77 K for n-type Bi_2Te_3.[a]

Sample	n_H	ρ_{11}	ρ_{123}	ρ_{312}	ρ_{1133}	ρ_{1122}	ρ_{1111}	ρ_{2223}
N1	0.252	11.7	19.3	32.8	25.4	11.5	8.54	5.70
N2	0.766	4.73	6.13	11.3	8.30	3.92	2.57	1.65
N3	2.57	2.19	1.88	3.77	2.29	1.01	0.745	...
N4	3.96	1.83	1.14	2.24	1.46	0.564	...	...
N5	4.10	1.70	1.24	2.37	1.36	0.586	0.443	0.288
N6	7.28	1.27	0.591	1.09	0.522	0.255	0.167	...
N7	9.70	1.10	0.402	0.763	0.299	0.154	0.107	0.066
N8	18.4	1.03	0.217	0.490	0.174	0.089	0.066	0.042
N9	19.2	1.01	0.201	0.417	0.137	0.056	0.035	...

[a] ρ_{11} is in units of 10^{-4} Ω cm, ρ_{123} is in cm^3/C, and ρ_{1133}, etc., are in units of 10^{-14} Ω cm/G^2. The carrier concentration n_H is given in units of 10^{18} cm^3.

ρ_{11}, ρ_{123}, ρ_{312}, ρ_{1111}, ρ_{1122}, ρ_{1133}, and ρ_{1123}.

In these experiments, the sample can be rotated independently of the magnetic field, as shown in Fig. 2. With this arrangement, all the components except one Hall coefficient are obtained in a single mounting of the sample. It is to be noted that the current $\vec{J}$ can be oriented arbitrarily with respect to the crystal axes in the basal plane. If ξ denotes the angle between $\vec{J}$ and the positive bisectrix, and d is the distance between the contacts a and b, then the magnetoresistance voltage V_{ab} will be

$$V_{ab} = JB^2 d(\rho_{2222}\cos^2\phi + \rho_{2233}\sin^2\phi + \rho_{2223}\sin 2\phi \cos 3\xi) , \quad (3)$$

for contacts on the cleavage surface and for $\theta = 90°$ in Fig. 2(a). We note that when $\theta = 90°$, the magnetoresistance voltage is due to $\rho_{2222} = \rho_{1111}$ for $\phi = 0$, and $\rho_{2233} = \rho_{1133}$ for $\phi = 90°$. Similarly, for $\theta = 0°$, $\rho_{2211} = \rho_{1122}$ is obtained for $\phi = 0°$, and ρ_{2233} for $\phi = 90°$.

From Eq. (3), it may be shown that the voltage as a function of field direction will be a minimum for a perfectly oriented crystal ($\xi = 0$) when

$$\tan 2\phi = -2\rho_{2223}/(\rho_{2233} - \rho_{2222}) . \quad (4)$$

Thus, since ρ_{2233} is larger than ρ_{2222}, as may be seen from Tables II and III, the minimum should lie between the $+3$ and -2 axes if ρ_{2223} is positive. The curve given by the open circles in Fig. 3, for a perfectly oriented crystal with $\theta = 90°$, illustrates this behavior. From the resulting value of ϕ, the off-diagonal coefficient ρ_{2223} may be determined. It should be noted that for $\theta = \xi = 0$ the magnetoresistance voltage is given by

$$V_{ab} = JB^2 d(\rho_{1122}\cos^2\phi + \rho_{2233}\sin^2\phi + \rho_{2213}\sin 2\phi) . \quad (5)$$

Since ρ_{2213} is equal to zero by symmetry, the maximum and minimum voltage should occur at values of ϕ corresponding to the crystal axes. This behavior is shown by the curve with the full circles in Fig. 3.

The sample holder, which can be rotated through approximately 180 deg by a spiral gear drive, is mounted between the poles of a 12-in. Varian magnet. Data are taken as a function of field for various angles θ and ϕ with a conventional measuring circuit, making use of an integrating digital voltmeter. The magnetoresistance coefficients are extracted from the raw data by a polynomial fit to the voltage V as a function of the field B, the maximum field at which Eq. (2) is valid being determined by the deviation from linearity in a plot of V vs B^2. In all cases care has been exercised to take a sufficiently high density of points in the low-field region corre-

TABLE III. Measured values of the magnetoresistance coefficients at 4.2 K for n-type Bi_2Te_3.[a]

Sample	n_H	ρ_{11}	ρ_{123}	ρ_{312}	ρ_{1133}	ρ_{1122}	ρ_{1111}	ρ_{2223}
N1	0.252	1.05	20.0	23.5	90.7	17.5	15.6	15.5
N2	0.766	0.437	7.84	9.44	31.2	6.16	5.10	5.47
N3	2.57	0.197	1.88	2.63	9.30	1.99	1.57	...
N4	3.96	0.171	1.17	1.77	7.77	1.68	1.50	...
N5	4.10	0.155	1.15	1.80	6.90	1.75	1.40	0.890
N6	7.28	0.190	0.620	1.15	3.42	1.07	0.776	...
N7	9.70	0.193	0.507	0.846	2.14	0.686	0.535	0.370
N8	18.4	0.208	0.277	0.517	0.966	0.322	0.238	0.184
N9	19.2	0.290	0.272	0.507	0.606	0.196	0.141	...

[a] See Table II for units.

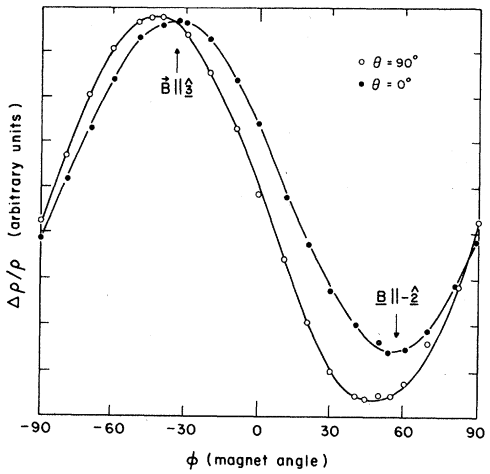

FIG. 3. Magnetoresistance $\Delta\rho/\rho$ vs field direction for sample $N5$ at 4.2 K. For $\theta=0$ the maximum of $\Delta\rho/\rho$ occurs along the trigonal axis and gives ρ_{1133}, while the minimum occurs along the bisectrix direction and gives ρ_{1122}.

sponding to $\omega\tau \ll 1$, ω being the cyclotron resonance frequency for the carriers in the field B.

IV. THEORY

A. Single-Band Magnetoresistance

The microscopic theory of the low-field magnetoresistance of Bi_2Te_3 can be simply calculated from the Boltzmann equation, assuming the six-ellipsoid model and an isotropic scattering time $\tau(E)$.[17] The transport equation is most readily solved in the principal-axis coordinate system for a representative ellipsoid, in which Eq. (1) becomes

$$E=(\hbar^2/2m)\,(\alpha_1 k_1'^2+\alpha_2 k_2'^2+\alpha_3 k_3'^2)\ . \tag{6}$$

Here α_i is the ith component of the inverse effective-mass tensor and k_i' is the corresponding components of the reduced wave vector, both referred to the principal axes. In this coordinate system, for example, the magnetoconductivity has the form

$$\sigma_{jklm}=\frac{e^4}{m_j m_k m_r}\,\frac{1}{2}(\epsilon_{rjm}\epsilon_{krl}+\epsilon_{rjl}\epsilon_{krm})\,[n\tau^3], \tag{7}$$

where, as usual, repeated indexes are summed, ϵ_{ijk} is the normal Levi-Cevita symbol, and $m_j=m/\alpha_j$ are the components of the effective mass in the principal-axis system. The brackets [ ] denote integration over the distribution

$$[n\tau^l]=\int_0^\infty \frac{2m^*E^{3/2}}{\hbar^2}\,\tau^l(E)\,\frac{\partial f(E)}{\partial E}\,dE, \tag{8}$$

where $f(E)$ is the Fermi-Dirac function and n is the carrier density in a given valley.

The total conductivity is evaluated by rotating the conductivity tensor for a single ellipsoid back to the crystal axes, and then adding together the conductivities of the six equivalent valleys. For the band structure given by (1), the principal axes are obtained by rotation about the $\vec{x}$ (or 1) axis in the sense $\vec{y}\times\vec{z}$ through an angle θ given by

$$\tan 2\theta=2\alpha_{23}/(\alpha_{22}-\alpha_{33})\ . \tag{9}$$

Following this procedure one finds, for example, that

$$\sigma_{1133}=(e^4/2m^3)\,[\alpha_{11}\alpha_{22}(\alpha_{11}+\alpha_{22})]\,[n\tau^3]\ . \tag{10}$$

The corresponding values of the magnetoresistance coefficients can then be obtained by inverting the tensor equations for the electric current in terms of $\vec{E}$ and $\vec{B}$.

B. Anisotropic Scattering Time

While the preceding analysis allows for the necessary anisotropy in the effective mass, it assumes an isotropic scattering mechanism. Herring and Vogt[18,19] and Korenblit[20] have shown that the solutions to the Boltzmann equation may be extended to the case of a relaxation time dependent on $\vec{k}$. The basic result is that the relaxation time becomes a tensor $\overleftrightarrow{\tau}$ and occurs only in the tensor product $\overleftrightarrow{\alpha}\cdot\overleftrightarrow{\tau}$. The tensor $\overleftrightarrow{\tau}$ may most conveniently be written

$$\overleftrightarrow{\tau}(E)=\phi(E)\begin{bmatrix}\tau_{11} & 0 & 0\\ 0 & \tau_{22} & \tau_{23}\\ 0 & \tau_{32} & \tau_{33}\end{bmatrix}, \tag{11}$$

where τ_{ij} is dimensionless, and it is assumed that the individual components of $\overleftrightarrow{\tau}$ all have the same energy dependence. It should be noted that $\overleftrightarrow{\tau}$ has the symmetry appropriate to the group of the electronic wave vector at the location of the energy minimum in $\vec{k}$ space. We shall always refer $\overleftrightarrow{\tau}$ to the principal-axis system of the carriers, holes or electrons. It should be noted that $\overleftrightarrow{\tau}$ is not diagonal in the same coordinate system as the effective-mass tensor and that τ_{23} does not, in general, equal τ_{32}.

Korenblit[20] has evaluated the conductivity tensor using this scheme, but the formulas are fairly unwieldly. We have found that the results for the conductivity tensor in the presence of an anisotropic scattering mechanism can be obtained directly from those for the isotropic case by making the following transformation:

$$\alpha_{11}'=\gamma_1\ ,$$

$$\alpha_{22}'=c^2\gamma_2+s^2\gamma_3-sc(\gamma_4-\gamma_5)\ ,$$

$$\alpha_{33}'=s^2\gamma_2+c^2\gamma_3+sc(\gamma_4-\gamma_5)\ ,$$

$$\alpha'_{23} = sc(\gamma_2 - \gamma_3) + c^2\gamma_4 - s^2\gamma_5 ,$$

$$\alpha'_{32} = sc(\gamma_2 - \gamma_3) + c^2\gamma_5 - s^2\gamma_4 , \tag{12}$$

where

$$\gamma_1 = \alpha_1\tau_{11}, \quad \gamma_2 = \alpha_2\tau_{22}, \quad \gamma_3 = \alpha_3\tau_{33}, \quad \gamma_4 = \alpha_2\tau_{23},$$

$$\gamma_5 = \alpha_3\tau_{32}, \quad \text{and} \quad c = \cos\theta, \quad s = \sin\theta$$

[θ is defined by Eq. (6)]. The extension to the case of anisotropic scattering, then, consists of merely replacing α_{ij} by α'_{ij} in formulas such as Eq. (10).

By applying the Onsager relations to the conductivity of a single ellipsoid, Korenblit has shown that $\alpha_2\tau_{23} = \alpha_3\tau_{32}$. Although this procedure seems incorrect, since the Onsager relations should hold for the total conductivity of the crystal and not necessarily for the conductivity of a single ellipsoid, Mackey and co-workers[21–23] have shown on more general grounds that the tensor product $\overleftrightarrow{\alpha} \cdot \overleftrightarrow{\tau}$ is symmetric (or, equivalently that $\gamma_4 = \gamma_5$). Consequently, in the subsequent analysis we shall assume $\alpha'_{32} = \alpha'_{23}$.

Aside from simplifying the theoretical expressions for the conductivity, the transformation given by Eq. (12) raises the question of precisely what information may be extracted from an analysis of magnetoresistance data. All the formulas for the conductivity tensor may be expressed in terms of the *four* α'_{ij}. There are, however, *five* "fundamental" quantities $\alpha_1\tau_{11}$, $\alpha_2\tau_{22}$, $\alpha_3\tau_{33}$, $\alpha_2\tau_{23}$, and $\sin\theta$, which contain direct information about the scattering and band structure. In general then, with an anisotropic scattering mechanism, magnetoresistance data alone will determine only the linear combinations of the fundamental quantities given by Eq. (12). At the same time, if the valley ellipsoids are not tilted or if the relaxation-time tensor is diagonal in the same coordinate system as the ellipsoids, the magnetoresistance can give direct information about the fundamental quantities.

A direct comparison of the experimental values of the transport coefficients with theory is not possible, since the product $\overleftrightarrow{\alpha} \cdot \overleftrightarrow{\tau}$ contains the factor $\phi(E)$ and, although theories exist for the energy dependence of the scattering time, the actual magnitude is not predicted. It is thus convenient to form *ratios* of the experimentally accessible coefficients, such as ρ_{312}/ρ_{123} and $\rho_{11}\rho_{1122}/\rho^2_{123}$, to overcome this problem. The formulas for these quantities, which involve only the ratios of α'_{ij} for the case of anisotropic scattering, are given in the Appendix.

For most of our samples the electrons and holes are degenerate ($E_F > k_BT$) at 77 K and all are highly degenerate for data taken at 4.2 K. In the single-band case, by forming the ratios given in the Appendix, the effects of incomplete degeneracy can be included in a single parameter

$$\beta = [n\phi^2]^2/[n\phi][n\phi^3] . \tag{13}$$

If it is assumed that

$$\phi(E) = bE^{-\lambda} , \tag{14}$$

the integrals in (13) may be evaluated for λ between -0.5 and 1.5 to give Fig. 4. Simple theories of impurity scattering give $\lambda = 1.5$, while for acoustic-phonon scattering $\lambda = -0.5$. At 77 K, the latter appears to be the dominant scattering mechanism and the value of β for our samples should be close to that given by Fig. 4 for $\lambda = -0.5$.

C. Two-Band Model

We have assumed that the second conduction-band minimum lies either at Γ or along ΓZ, since this is the prediction made by the band-structure calculations.[14] The inverse effective-mass tensor for the second-band minimum referred to the crystal axes is then

$$\overleftrightarrow{\delta} = \frac{1}{m}\begin{pmatrix} \delta_1 & 0 & 0 \\ 0 & \delta_1 & 0 \\ 0 & 0 & \delta_3 \end{pmatrix} , \tag{15}$$

while the relaxation-time tensor for electrons in the second band will have the same form. The total conductivity is obtained by summing the contributions for the two bands, to give for our previous example

$$\sigma_{1133} = (e^4/2m^3)\{[n_l\tau_l^3]_l\alpha_{11}\alpha_{11}(\alpha_{11} + \alpha_{22}) + 2[n_u\tau_u^3]_u\delta_1^3\} , \tag{16}$$

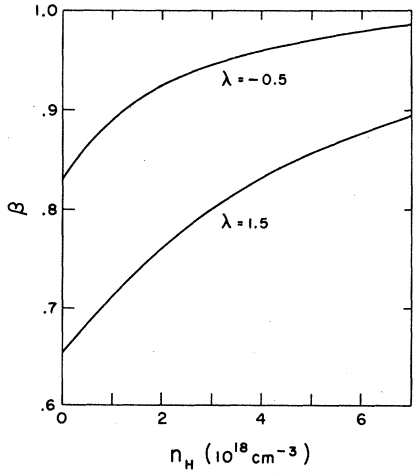

FIG. 4. Plot of parameter β as a function of the carrier concentration for two different values of λ corresponding to phonon and impurity scattering. The calculations assume $m^* = 0.101m$ and that the second band begins to fill at a Fermi energy of 24.5 meV relative to the bottom of the first band.

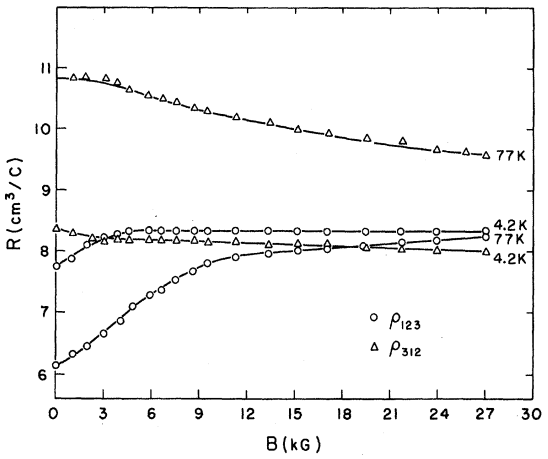

FIG. 5. Variation of the two Hall constants ρ_{123} and ρ_{312} as a function of magnetic field for sample $N2$. At 4.2 K and high fields, the constants saturate to the same value within 5%.

where the subscripts l and u indicated lower and upper band, respectively. The integration denoted $[\,]_u$ is identical to that of Eq. (8) except that the appropriate Fermi energy to use in the Fermi-Dirac function is $E_F - E_0$, E_0 being the energy at which the second band starts to fill.

For the two-band model, it is most convenient to use the same experimental ratios as for the single-band case; the formulas are given in the Appendix. The quantity $P = n_u/n_l$ is factored out, since it can be determined from a combination of dHvA or Shubnikov-de Haas (SdH) and Hall data. At helium temperatures, the electrons in both bands are degenerate and the integrals such as $[n\tau^3]_u$ become $n_u\phi_u^3$ [where ϕ_u means $\phi_u(E)$ evaluated at $E_F - E_0$]. In this case, Q and P become direct ratios of the two mobilities of the upper band, $e\delta_1\tau_{11}\phi_u$ and $e\delta_3\tau_{33}\phi_u$, to the mobility component $e\alpha'_{22}\phi_l$ for the lower band. At 77 K we have assumed that the electrons in the first band are degenerate (the second band does not start to fill until $E_F/k_BT > 5$ for the first band) and we have calculated the correction factors I_j to take account of the incomplete degeneracy in the second band at 77 K. The above analysis applies to both valence and conduction bands with only changes in notation.

V. EXPERIMENTAL RESULTS AND DISCUSSION

A. n-Type Bi_2Te_3

Tables II and III contain the results of the magnetoresistance measurements on n-type samples, all of which are tellurium doped with the exception of sample $N9$ which is doped with iodine. The data of Drabble[1] and Goldsmid,[24] which refer to iodine-doped samples, are included in the tables along with the results of Caywood[25] on tellurium-doped samples. The carrier concentrations have been determined from the average of ρ_{123} and ρ_{312} at 4.2 K for a field of 30 kG. In this high-field limit, $\omega\tau \gg 1$ and the two Hall coefficients saturate to the same value R, which is related to the carrier density n_H by the expression

$$R = 1/n_H e \,. \tag{17}$$

An example of this limiting behavior is shown in Fig. 5. Since high-field Hall data are not available for the samples of other workers, the relevant carrier concentrations have been determined by comparing the average of ρ_{123} and ρ_{312} at low fields to the same averages from our data.

Figure 6 shows the results for the most easily measured transport coefficient ρ_{11} at 77 and 4.2 K. The data, particularly at 4.2 K, exhibit an unusual dependence on carrier concentration. For carrier densities less than 3×10^{18} cm^{-3}, the resistivity decreases with increasing carrier concentration in agreement with the dashed line, which has been calculated from the simple one-band model. However, for n above 3×10^{18} cm^{-3}, the decrease is negligible and eventually the resistivity begins to increase with increasing carrier density. The most plausible explanation of this effect is the reduction in total electronic mobility possible with a second band of sufficiently heavy mass, or low mobility. As impurities are added, the Fermi energy increases to the point where the second heavy-mass band begins to fill. Due to the heavy mass and hence the large density of states in the second band, the majority of the additional electrons go into the low-mobility band as more impurities are added. The presence of the second band alone would explain the data at 77 K. However, at 4.2 K the resistivity is due to impurity scattering, and there is a reduc-

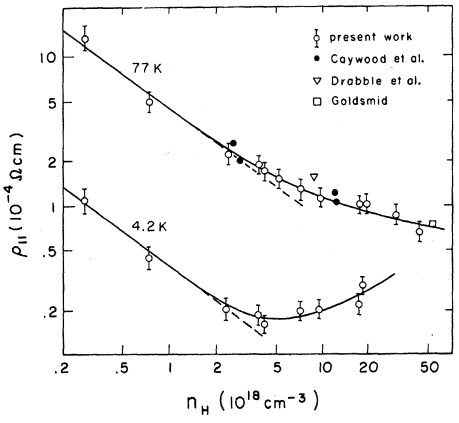

FIG. 6. Resistivity of n-type Bi_2Te_3 as a function of carrier concentration at 77 and 4.2 K. Deviations from the dashed lines, which are the predicted behavior of the simple one-band model, are attributed to the effects of a second set of conduction-band minima.

tion of the mobility of the first band above a carrier density equal to 4×10^{18} cm^{-3}. With the addition of impurities, whose donor electrons go into the heavy-mass ($m^*=1.5m_0$)[5] band, the net effect is to add ionized impurities to the crystal. The relatively immobile electrons of the second band will not screen the impurity atoms as well as the electrons in the lower band screen their donor atoms. Consequently, the mobility of the electrons in the lower band is also reduced because of the increased number of scattering centers. This explains, in part, the weakness of dHvA and SdH oscillations for samples with carrier density in excess of 4×10^{18} cm^{-3}.

The band structures of GaSb and grey tin are similar to that of Bi_2Te_3 in that they also possess a second heavy-mass band, which can be populated by suitable doping. However, the behavior of their electronic mobility with increasing carrier concentration is strikingly dissimilar to the results reported in this work. Specifically, in both materials the mobility of the lower band increases when the second band begins to fill[26,27] and the SdH oscillations are enhanced by increased doping.

Robinson and Rodriguez[28] have advanced a theory, based on the band parameters of GaSb, which shows that the screening length for ionized impurities *decreases* when the Fermi level reaches the second-band minimum. This theory cannot be applied to the case of Bi_2Te_3 without first taking into account the following complications. First, the ratio of the upper- to lower-band masses is two orders of magnitude smaller than in GaSb, while the energy separation of the two bands is a factor of 3 smaller. Second, the effective-mass and relaxation-time tensors are highly anisotropic in

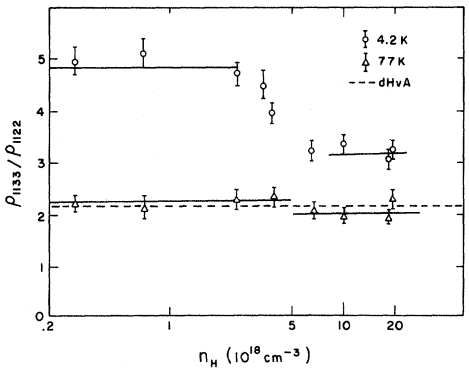

FIG. 7. Variation with carrier density of the ratio ρ_{1133}/ρ_{1122} for n-type Bi_2Te_3 at 77 and 4.2 K. The dashed line is the prediction of the single-band model, using the dHvA band parameters and assuming an isotropic relaxation time. Deviations from the predicted behavior are attributed to anisotropy of the scattering time and the effects of a second band.

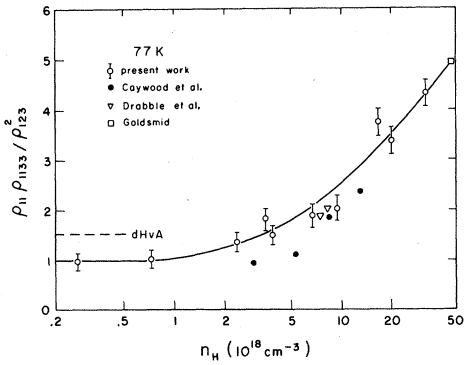

FIG. 8. Variation with carrier density of the ratio $\rho_{11}\rho_{1133}/\rho_{123}^2$ for n-type Bi_2Te_3 at 77 K. The dashed line is the prediction of the single-band model, using the dHvA band parameters and assuming an isotropic relaxation time. Deviations from the predicted behavior are attributed to anisotropy of the scattering time and the effects of a second band.

Bi_2Te_3, whereas, the above-mentioned theory assumes both to be isotropic. Finally, the intervalley contribution to the scattering can be neglected in the case of GaSb,[28] while the same assumption may not be valid here. Thus, it is not clear whether the theory does in fact predict a similar decrease for the scattering by ionized impurities in Bi_2Te_3 when the second band begins to fill.

Figure 7 shows the ratio ρ_{1133}/ρ_{1122}, which is the most accurately determined magnetoresistance parameter. Both the coefficients ρ_{1133} and ρ_{1122} are large and any uncertainties in measurement of sample area and contact separation do not enter the ratio ρ_{1133}/ρ_{1122} for a given experiment. In the single-band model it is independent of carrier concentration. Reference to Fig. 7 shows that although the ratio is indeed constant at 77 and 4.2 K for both low and high carrier densities, there is a sharp break in the latter data for n approximately equal to 4×10^{18} cm^{-3}. This behavior constitutes the most direct evidence from the present work for the existence of a second band. The dashed line is the value of the ratio ρ_{1133}/ρ_{1122} predicted from the dHvA data in Table I, assuming an isotropic scattering mechanism. The large disagreement at 4.2 K, particularly in the region where only one band is contributing, indicates considerable anisotropy in the scattering time for electrons. Figure 7 also indicates that the anisotropy of the phonon scattering at 77 K is apparently small compared to impurity scattering.

Figures 8 and 9 show the ratio $\rho_{11}\rho_{1133}/\rho_{123}^2$ and the value predicted by the dHvA band parameters. This ratio depends on carrier concentration only through the degeneracy parameter β, which increases with increasing carrier concentration, the lowest value being equal to 0.6 for sample $N1$

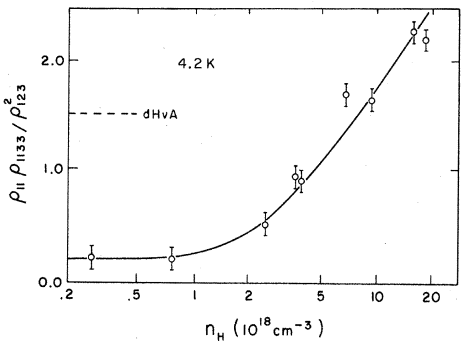

FIG. 9. Variation with carrier density of the ratio $\rho_{11}\rho_{1133}/\rho_{123}^2$ for n-type Bi_2Te_3 at 4.2 K. The dashed line is the prediction of the single-band model, using the dHvA band parameters and assuming an isotropic relaxation time. Deviations from the predicted behavior are attributed to anisotropy of the scattering time and the effects of a second band.

at 77 K. From Eq. (A1), it is clear that the ratio decreases with increasing β, so that the variation in Figs. 8 and 9 is most easily attributed to the effects of the second band. For reasonable values of the second-band parameters and for u greater than unity, the derivative of D with respect to P is positive. Consequently, the two-band model predicts that $\rho_{11}\rho_{1133}/\rho_{123}^2$ will increase with increasing carrier concentration (n_u/n_l always increases with increasing n_H), in agreement with experiment. Like ρ_{1133}/ρ_{1122}, the ratio $\rho_{11}\rho_{1133}/\rho_{123}^2$ is relatively constant at low carrier concentrations, and the agreement with the dHvA prediction is better at 77 than at 4.2 K.

The importance of determining the sign of ρ_{2223}, as well as the magnitude, can be seen from Eq. (A1). The parameter α_{23} (or α'_{23} in the anisotropic theory) enters the expression for ρ_{1123} to the first power, whereas all other ratios involve w or α_{23}^2. As can be seen from Fig. 3, our data gives ρ_{2223} as positive for all the samples or equivalently $\rho_{1123} < 0$. Thus, for u greater than unity, as is the result of our data analysis, α_{23} determined from the magnetoresistance data is positive at both 4.2 and 77 K, in agreement with the dHvA data.

B. p-Type Bi_2Te_3

Tables IV and V show the results of measurements on p-type Bi_2Te_3. The carrier concentrations have been determined in the same manner as described for n-type samples, with the exception that the data have been extended to higher fields (50 kG) to achieve what appeared to be saturation behavior.

Figure 10 shows ρ_{11} at both temperatures, including the data of Drabble and Efimova. Although the behavior is similar to that of n type, the features attributed to two-band behavior in n type are not as distinct for p type, perhaps due to the more limited range of hole concentrations studied. Figure 11 shows the ratio $\rho_{11}\rho_{1133}/\rho_{123}^2$ for p type and the same comments are generally applicable. Namely, the ratio would be expected to remain constant with carrier concentration if there is only a single band, as has been proposed by both Testardi and Efimova.

VI. ANALYSIS

To analyze the magnetoresistance data in terms of the models of the band structure, it is necessary to solve Eqs. (A1) and (A2) knowing the experimental ratios A, B, C, D, E, and F. For the single-band case, it is possible to obtain the relevant parameters u, v, w, and β from four experimental ratios, as shown in the Appendix. In this work, for both the one- and two-band cases, an optimization procedure has been used to fit all *six* experimental ratios by varying the appropriate band parameters. This procedure is similar to that used recently in an analysis of the low-temperature transport properties of bismuth.[29]

The solutions are constrained by the theory to have u, v, Q, and R greater than zero and $v > w$ (since $v - w = \alpha_{23}^2/\alpha_{22}^2$). For almost every sample studied, there exist two distinct sets of solutions

TABLE IV. Measured values of magnetoresistance coefficients at 77 K for p-type Bi_2Te_3.[a]

Sample	p_H	ρ_{11}	ρ_{123}	ρ_{312}	ρ_{1133}	ρ_{1122}	ρ_{1111}	ρ_{2223}
*P*1	0.920	5.72	4.43	7.90	30.5	13.4	11.2	5.06
*P*2	1.45	3.29	2.59	4.51	17.2	8.31	6.54	1.32
*P*3	2.10	3.07	1.85	3.32	12.9	7.09	5.94	•••
*P*4	10.0	1.49	0.289	0.686	1.21	0.685	0.639	•••
*P*5	10.6	1.41	0.275	0.676	1.22	0.672	0.636	0.586
*E*1[b]	14.2	1.47	0.230	0.460	0.775	0.355	0.357	•••
*D*19[c]	3.45	4.23	1.06	2.16	3.44	1.66	1.25	•••
*D*23[c]	12.8	1.40	0.240	0.570	0.840	0.495	0.425	•••

[a] ρ_{11} is in units of 10^{-4} Ω cm; ρ_{123} and ρ_{312} are in cm^3/C; ρ_{1133}, etc., are in units of 10^{-13} Ω cm/G^2; p is in units of 10^{18} cm^{-3}.

[b] See Ref. 9.

[c] See Ref. 2.

TABLE V. Measured values of magnetoresistance coefficients at 4.2 K for p-type Bi_2Te_3.[a]

Sample	p_H	ρ_{11}	ρ_{123}	ρ_{312}	ρ_{1133}	ρ_{1122}	ρ_{1111}	ρ_{2223}
$P1$	0.920	1.17	4.97	7.65	82.5	29.4	28.5	9.0
$P2$	1.45	0.540	2.86	3.97	81.8	20.2	19.0	3.0
$P3$	2.10	0.548	1.87	2.88	51.6	16.7	14.5	•••
$P4$	10.0	0.521	0.234	0.635	2.50	1.26	1.34	•••
$P5$	10.6	0.536	0.222	0.581	2.08	1.29	1.08	0.685
$E1$[b]	14.2	0.665	0.212	0.416	1.32	0.545	0.567	•••

[a]See Table IV for units.

[b]See Ref. 9.

which satisfy the constraints: One set has $u > 1$ (actually ranging between 4 and 10) and the other has $u \simeq 0.1$. We will refer to them as solutions I and II, respectively. It is not strictly possible to determine which solution is the "correct" solution on the basis of the magnetoresistance data alone. However, in the subsequent analysis we shall discard the solutions $u = 0.1$ for the following reasons. First, for three of the samples it is not possible to obtain a fit with solution II which satisfies the constraint $u > w$. Second, solution I gives the "best" fit in most cases, although for some samples the solutions are indistinguishable from this criterion. Finally, the dHvA (for both n- and p-type) data predict $u = 8.0$, and solution II requires an extremely large anisotropy in $\overline{\tau}$ to give a value of 0.1 for u. In this regard, Herring[18] questions the validity of the usual solutions to the Boltzmann equation with large anisotropies in $\overline{\tau}$.

Tables VII and VIII show the results of the fitting program for a low- and high-concentration n-type sample and a p-type sample. The fits obtained for the six experimental qualities in terms of only u, v, and w are extremely good for the low carrier-concentration samples at both 4.2 and 77 K. (β is allowed to vary in fitting the 77-K data for low-carrier-concentration samples.) For n greater than 4×10^{18} cm^{-3}, the two-band model satisfactorily fits the experimental results, using the values of P and I_1, I_2, and I_3 given in Table VI, and the parameters u, v, w, Q, and R given in Tables VII and VIII.

The parameter $F = (\rho_{123} + \rho_{312})n$, appearing in Tables VII and VIII, incorporates our knowledge of the carrier concentration from the high-field Hall and dHvA data into the analysis of the low-field magnetoresistance. In the degenerate case we may write for the single-band model [see Eqs. (A1) and (A2)]

$$\rho_{ijk} = (1/ne)\, q(u, v, w)\,, \tag{18}$$

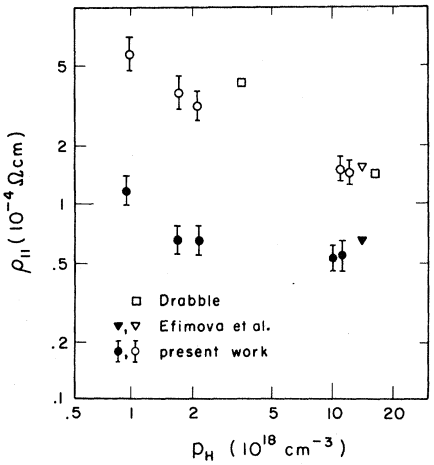

FIG. 10. Resistivity of p-type Bi_2Te_3 as a function of carrier concentration at 77 and 4.2 K. The open points are data taken at 77 K, while the solid points are data taken at 4.2 K.

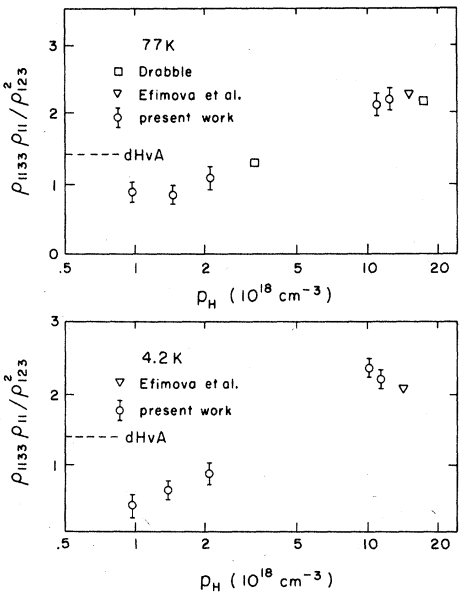

FIG. 11. Variation with carrier density of the ratio $\rho_{11}\rho_{1133}/\rho_{123}^2$ for p-type Bi_2Te_3 at 77 and 4.2 K. The dashed line is the prediction of the single-band model for the valence band, using the dHvA band parameters and assuming an isotropic relaxation time.

TABLE VI. Values of E_F, P, and I_j used in calculations of β and the two-band analysis.[a]

Sample	n_H	n_E	E_F	P	I_1	I_2	I_3
*N*6	7.28	5.2	33.0	0.39	1.55	0.943	0.680
*N*7	9.70	5.8	35.1	0.69	1.38	0.923	0.711
*N*8	18.4	7.3	41.2	1.50	1.08	0.913	0.858
*N*9	19.2	7.4	41.5	2.02	1.07	0.911	0.861

[a]Both n_H and n_E are in units of 10^{18} cm^{-3}, while E_F is in meV.

where q is a function only of the parameters u, v, and w. The carrier density n is determined from the average of the high-field data, i.e., $n_H = \frac{1}{2}(\rho_{123}+\rho_{312})_{HF}$, so that by forming the ratio $F = 2(\rho_{123}+\rho_{312})/(\rho_{123}+\rho_{312})_{HF}$ we obtain a dimensionless quantity, which is a function of the anisotropy parameters only. This is equivalent to predicting the high-field Hall-constant average from the low-field data alone. The full curve in Fig. 12 shows the predicted variation of F with carrier concentration obtained from a fit of the single-band model to the values of $A-E$ for the n-type samples. There is clearly a discrepancy with the open points computed from $(\rho_{123}+\rho_{312})n_H$, which indicates that the number of carriers determining the low-field coefficients is considerably less than n_H. This result indicates the existence of a second conduction band independent of the dHvA data. It is noteworthy that, on the basis of the present work, this second band begins to populate at a significantly lower carrier density than previous estimates, viz., approximately 2×10^{18} cm^{-3}.

A substantially better fit to the computed value of F is obtained if, instead of n_H, one uses the values of n_E computed from dHvA data. The resulting behavior is shown by a comparison of the full curve with the triangles in Fig. 12. At low carrier densities, the fit is unchanged, since $n_E = n_H$ in this regime. Finally, the dashed line in Fig. 12 gives the computed behavior of F using the parameters obtained from a two-band fit to experimentally determined ratios $A-E$. The agreement between the experimental and computed values of F is satisfactory and indicates that the fitting parameters give an accurate description of the available experimental data.

TABLE VII. Experimental and fitted values of the parameters for Bi_2Te_3 at 4.2 K.

	Sample	A	B	C	D	E	F
	measured	1.17	0.041	0.046	0.238	0.041	1.77
*N*1	predicted	1.21	0.045	0.042	0.231	0.043	1.80
	measured	1.66	0.402	0.514	1.61	0.279	(1.15, 2.10)[a]
*N*7	predicted	1.82	0.337	0.561	1.49	0.289	0.984
	measured	2.62	1.17	1.40	2.26	0.745	0.955
*P*3	predicted	2.64	1.05	1.58	2.24	0.774	1.02

[a]Values obtained from n_E and n_H, respectively.

TABLE VIII. Values of parameters used in obtaining best least-squares fit to transport properties of Bi_2Te_3 at 4.2 K.

Sample	u	v	w	P	Q	R
*N*1	2.53	0.425	0.399	0	•••	•••
*N*7	7.57	0.739	0.646	0.680	0.705	0.560
*P*3	10.9	1.58	1.25	0.300	1.04	1.29

The parameters u, v, and w, deduced from analysis of the low-field transport properties, should determine the tensor product $\overleftrightarrow{\alpha}\cdot\overleftrightarrow{\tau}$ as explained in Sec. IV. We have used the values of α_{ij} from the dHvA data to determine the anisotropy ratios τ_{22}/τ_{11}, τ_{33}/τ_{11}, and τ_{23}/τ_{11} from the transformation (A9). These values are shown in Fig. 13. Since it is clear from the data that $\tau_{23}\neq 0$ (although it is small for phonon scattering), the magnetoresistance data cannot alone be used to determine anything but $\alpha'_{11}/\alpha'_{22}$, etc. Previous workers have determined u, v, and w from the low-field data and have attempted a comparison directly[25] with the dHvA parameters. Alternatively, it has been assumed that τ_{23} is zero[9] to give values for $\alpha_2\tau_{22}/\alpha_1\tau_{11}$. Neither procedure appears to have been correct.

The analysis of the data for p-type Bi_2Te_3 is less straightforward. Although the experimentally determined ratios for samples $P1$, $P2$, and $P3$ can be

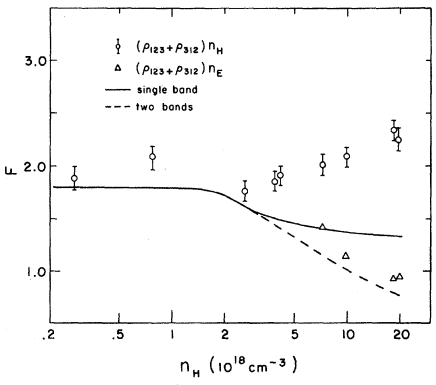

FIG. 12. Variation with carrier density of the parameter $F = (\rho_{123}+\rho_{312})n$ for n-type Bi_2Te_3 at 4.2 K. The full curve is the predicted behavior with the parameters $A-E$ using a single-band model, while the dashed curve is the calculated behavior using a two-band model. The circles and triangles show the experimental values of F using n_H and n_E, respectively, for the carrier density.

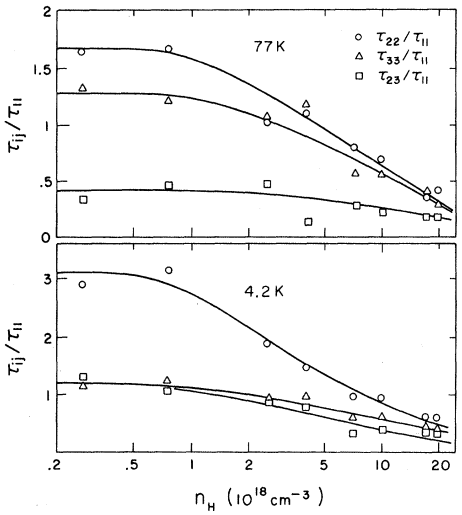

FIG. 13. Dependence on carrier density of the components of τ_{ij}/τ_{ii} for n-type Bi_2Te_3 at 77 and 4.2 K.

fitted individually to the single-band model very well, the resulting anisotropy parameters u, v, w are not the same for the different samples. The difficulty appears to be associated with the parameter α'_{23} [or $(v-w)^{1/2}$]. The component ρ_{1123} is directly proportional to α'_{23}, as discussed previously, and our measurements on $P2$ and $P3$ indicate that ρ_{1123} is too small to be measured accurately. It may be shown that if the magnetoresistance in the basal plane is isotropic, then v must equal w, or $\alpha'_{23}=0$. In this respect, the experimental data are consistent, since the parameters ρ_{1122} and ρ_{1111} are virtually the same and ρ_{1123} is nearly equal to zero (as must be the case if $\alpha'_{23}=0$). The result is that v and w are quite sensitive to slight variations of ρ_{1123} or to the relative magnitudes of ρ_{1122} and ρ_{1111}.

An additional difficulty is encountered when using the transformation given by Eq. (A9) in conjunction with the dHvA data to obtain τ_{ij}/τ_{11} from u, v, and w. The dHvA results give α_{23} negative while our low-field data at 4.2 K indicates that α'_{23} is positive. The sign of α'_{23} determines whether $(v-w)^{1/2}$ is taken to be positive or negative in Eq. (A9), while the sign of α_{23} determines the sign of the tilt angle. SdH data have been taken on sample $P2$ at the same time as the low-field magnetoresistance data, and our high-field results confirm that the sign of α_{23} is negative, as originally presented by Testardi. Thus, it would appear that τ_{23} is negative, which does not appear to be physically reasonable. However, since the coefficient is quite small, its value has been assumed to be zero.

As might be expected, the ratio τ_{22}/τ_{11} is not affected by these difficulties and is relatively the same for all three samples. However, τ_{33}/τ_{11} and τ_{23}/τ_{11} vary to such an extent between the samples that we have chosen to use only the results for $P2$, since this is the most extensively studied sample as well as the most favorably aligned. The results are $\tau_{22}/\tau_{11}=2.00$ and 2.55; $\tau_{33}/\tau_{11}=1.13$ and 0.847; $\tau_{23}/\tau_{11}=0.248$ and 0 for 77 and 4.2 K, respectively. Samples $P1$ and $P3$ give results for τ_{33}/τ_{11} and τ_{23}/τ_{11} differing from those quoted by nearly 50% (τ_{33}/τ_{11} for $P1$ and $P3$ is less than the above, τ_{23}/τ_{11} greater).

To complete a two-band analysis of a sample with $P_H=10.6\times10^{18}$ cm^{-3}, it is necessary to determine the hole concentration in the higher valence band. From SdH data taken on this sample in fields up to 30 kG, the hole density is found to be 7.2×10^{18} cm^{-3}, giving $P(=p_u/p_l)$ equal to 0.47. Using this value, one obtains $Q/R=1.73$ and 0.81 for 77 and 4.2 K, respectively. The relaxation times are found to be $\tau_{22}/\tau_{11}=1.62$ and 1.25; $\tau_{33}/\tau_{11}=0.200$ and 0.390; $\tau_{23}/\tau_{11}=0.760$ and 0.491 for 77 and 4.2 K, respectively.

VII. DISCUSSION

The discrepancy between the band parameters for n-type Bi_2Te_3 obtained from dHvA[4] and previous magnetoresistance measurements[3] has been attributed to the fact that the original analysis of the transport properties effectively ignored one of the solutions to Eq. (A6).[25] However, these magnetoresistance data have been obtained at 77 K for samples doped such that a significant fraction of the carriers occupy states in the upper conduction band. An explanation of the results in terms of a single band requires a value of β equal to 0.7 for a carrier concentration of approximately 10^{19} cm^{-3}. It is clear from Fig. 7 that such a low β is not consistent with any simple model of the relaxation mechanism. In addition, the dependence of the transport coefficients on carrier concentration shown in Figs. 9–12 cannot be reconciled in any convincing way with the single-band analysis. The success of the two-band model, with assumed anisotropy in the scattering processes, in explaining all the available data must be regarded as demonstrating its essential correctness.

Some general comments can be made about the anisotropies in $\overleftrightarrow{\tau}$. It is not clear how the presence of available states in the second band will affect the scattering time of the electrons in the first band. Therefore, the results for low carrier concentrations should be considered as representative of the scattering times for impurities and phonons, rather than the results for n greater than 4×10^{18} cm^{-3}. At 77 K, there will be a population of the second band due to thermal excitation, even for samples with n less than 4×10^{18} cm^{-3}. Consequently, the results for $N3$ and $N5$ at 77 K may not be correct, since the effects of thermal population of the upper band have not been considered.

The only existing theory predicting τ for either impurity or phonon scattering has been formulated by Korenblit[20] for the acoustic-phonon case. This theory has τ_{22}/τ_{11} and τ_{33}/τ_{11} of order unity, and τ_{23}/τ_{11} nearly an order of magnitude smaller. Although our data at 77 K give τ_{23}/τ_{11} considerably smaller than the other ratios, the detailed lack of agreement with the predicted behavior probably indicates that other processes, such as intervalley scattering, are important. The Debye temperature for Bi_2Te_3 is 165 K, so that there will be a significant fraction of the excited phonon modes able to scatter electrons between different minima, regardless of their position in $\vec{k}$ space. Herring[18] has pointed out that intervalley scattering should be an isotropic process since the momentum of the initial and final electron states, relative to the band edge, will be small compared to the change of momentum involved in the scattering. The results at 77 K shown in Fig. 13 can therefore be expected to represent a mixture of isotropic and anisotropic scattering. It should be noted, however, that the argument about intervalley scattering will be modified by the highly anisotropic nature of the acoustic properties of Bi_2Te_3.[30] Therefore, the isotropic component may be relatively small.

The results of the two-band analysis for $N6$–$N9$ at 77 K are particularly simple. Without constraining the variables Q and R in any way, the result $Q = 1.40 \pm 0.10$ and $R = 1.05 \pm 0.15$ is found to give the best fit for all samples. Consequently, for phonon scattering $\delta_1\tau_{11}''/\delta_3\tau_{33}'' = 1.40$, so that it is probable that the effective-mass parameters of the second band are not highly anisotropic. At 4.2 K, Q and R vary in magnitude as a function of carrier concentration, but their ratio Q/R is approximately equal to 1.10 for all the samples. Both Q and R (which are actually ratios of second-band mobilities to first-band mobilities) are found to decrease with increasing carrier concentration. The most surprising aspect of the two-band analysis is that the mobility in the second band, while lower than that of the first band, is not as small as would be expected from its high effective mass $m^* = 1.5m$.[5]

The second band has a noticeable effect on the anisotropy parameters deduced for the first band. It is impossible to fit the data by requiring that u, v, and w be the same as those obtained for the low-concentration samples and varying only the upper-band parameters Q and R. This result could be due either to an effect on the relaxation rates of the lower-band electrons caused by the second-band states at the Fermi level or to an incorrect choice for the location of the second-band minima. Should the subsidiary minima lie not at Γ or along ΓZ but rather in a mirror plane, a correct characterization of the second band would require two additional parameters if the ellipsoids are tilted (or one parameter if they are not). The formulas for such a model are quite cumbersome and the regularity of our results, combined with the predictions of the band-structure calculations, indicates that a more complex model is not required at present.

Whatever the location of the second-band minimum, the possible effects on the scattering times of the first band must be considered. We have previously mentioned that the impurities, whose electrons occupy states in the heavy-mass band, will effectively increase the number of centers scattering the lower-band electrons. There is no apparent reason why the anisotropy of the relaxation-time tensor should be affected merely by increasing the number of scattering centers. However, if the Fermi level is raised to a point such that states in both bands are occupied, the possibility of interband scattering cannot be ignored. In our model the two bands do not overlap in $\vec{k}$ space, but at 77 K there are phonons excited which can scatter electrons between separated minima, and consequently, between states in different bands. Since the effective masses of the two bands differ by a factor of more than 10, this process would certainly cause the relaxation times to differ from the phonon relaxation times obtained for a single band.

Another possible effect influencing the relaxation rates is electron-electron scattering. As the number of electrons in the heavy-mass band increases, one would expect this effect to become more important, but it is difficult to estimate the magnitude of electron-electron scattering relative to the other scattering processes. Since the relaxation time approximation and the usual solutions of the Boltzmann equation are not valid for electron-electron scattering, it is not clear how this process would manifest itself in our data.

Although the data for p-type Bi_2Te_3 are also consistent with a two-band model, the results are less satisfying than for n type. A source of some difficulty may be that the second valence-band maximum does not lie at Γ or along ΓZ. However, an analysis based on a more complex model should be accompanied by an increase in the number of experimentally determined quantities (it appears possible to measure ρ_{33}, ρ_{3333}, and ρ_{3311} for p-type crystals). The effective-mass parameters and location of the second valence-band maximum have only been discussed briefly in the available literature. When more detailed knowledge of the band parameters is available, a comparison of the scattering parameters deduced from the transport data presented here for n and p type should prove interesting.

VIII. CONCLUSIONS

The experimentally determined transport coefficients for n-type Bi_2Te_3 have been explained in terms of a single-band model for low carrier con-

centrations and a two-band model for higher concentrations. The three parameters used to describe the anisotropy of the lower band have been combined with the dHvA parameters to deduce the anisotropies of the relaxation-time tensor. The scattering anisotropies obtained at 4.2 K for the low-concentration samples should provide a useful test for any calculation of impurity scattering in rhombohedral materials. It is apparent from our results that the off-diagonal term τ_{23} is considerable for impurities and must be considered in future analyses or theories.

There are two likely methods for resolving the discrepancy between our results and the existing theory of phonon scattering. One possibility is an extension of Korenblit's theory to include intervalley scattering. However, such an extension may only be possible under the usual simplifying assumption that the energy loss suffered by an electron in a collision amounts to a small fraction of its total energy. Since the phonon energies at 77 K involved in intervalley scattering may amount to 20% of the electron energy, it would be desirable to extend the measurements to temperatures below 77 K. By performing measurements, such as those reported here, as a function of temperature it should be possible, after eliminating the temperature-independent terms due to impurities, to determine the inter valley and intravalley contributions to the scattering.

The two-band model used here assumes the location of the subsidiary minima to be at Γ or along ΓZ. Our analysis indicates the upper band to be relatively isotropic, with a mobility larger than expected on the basis of the calorimetric data. Attempts have been made to observe oscillations in the dHvA or SdH data due to the second band, but as yet these attempts have been unsuccessful. It would, of course, be advantageous to have direct information about the second band, such as effective-mass parameters or its location in $\vec{k}$ space. However important it may be to obtain more information concerning the second band, it seems clear that a better understanding of the important transport properties requires further work on the nature of the electronic scattering processes.

ACKNOWLEDGMENTS

The authors would like to acknowledge useful discussions with Dr. R. Hartman, Dr. P. Drath, Dr. D. Sellmyer, Dr. J. Mackey, and Dr. J. Melngailis. Thanks are also due to J. Barnes and T. Davis for their help in performing some of the experiments. This work has been supported by the National Science Foundation.

APPENDIX

For the case of a single-band and an isotropic scattering mechanism, the ratios $A=\rho_{312}/\rho_{123}^2$, $B=\rho_{11}\rho_{1111}/\rho_{123}^2$, $C=\rho_{11}\rho_{1122}/\rho_{123}^2$, $D=\rho_{11}\rho_{1133}/\rho_{123}^2$ and $E=\rho_{11}\rho_{1123}/\rho_{123}^2$ are given by the equations

$$\begin{aligned}
A &= (uv+w)(1+u)/4uv\ ,\\
B &= [w(1-5u)+uv(3+u)](1+u)/16\beta u^2\ ,\\
C &= [w(3+u)+uv(1+3u)](1+u)/16\beta u^2 - 2A^2v/(1+u)\ ,\\
D &= (1+u)^2/4\beta u - 1\ ,\\
E &= -\alpha_{23}(u^2-1)/8\beta u\ ,
\end{aligned} \tag{A1}$$

where $u=\alpha_{11}/\alpha_{22}$, $v=\alpha_{33}/\alpha_{22}$, $v-w=\alpha_{23}^2/\alpha_{22}^2$, and β is defined in Eq. (13). For the case of anisotropic $\overleftrightarrow{\tau}$, $u=\alpha'_{11}/\alpha'_{22}$, $v=\alpha'_{33}/\alpha'_{22}$, and $v-w=\alpha'^2_{23}/\alpha'^2_{22}$, where the α'_{ij} are given in Eq. (12).

We define the parameter $F=(\rho_{123}+\rho_{312})n$, where n is determined from the high-field Hall or dHvA data. Using the relations

$$\begin{aligned}
\rho_{123} &= \frac{4[n\tau^2]u}{[n\tau]^2(1+u)^2}\ ,\\
\rho_{312} &= \frac{[n\tau^2](uv+w)}{[n\tau]^2(1+u)v}\ ,
\end{aligned} \tag{A2}$$

it is easily shown that

$$F=\{4uv+(1+u)(uv+w)\}/v(1+u)^2\ . \tag{A3}$$

For $E_F \gg k_BT$, $[n\tau^2]/[n\tau]^2 = 1/n$, and for data taken at 77 K, the integrals have been numerically evaluated to give a corrected value of F to use in the fitting procedure.

For the two-band model, assuming that the electrons or holes in the lower band are degenerate, the ratios can be written as

$$\begin{aligned}
A &= (w+uv+2I_2PQR)U_p/4V_pU_m\ ,\\
B &= [uv(3+u)+w(1-5u)]U_p/16U_m^2\ ,\\
C &= [uv(3u+1)+w(3+u)+8I_3PQ^2R]\\
&\qquad \times U_p/16U_m^2 - 2A^2V_p/U_p\ ,\\
D &= U_p[u(u+1)+2I_3PQ^3]/4U_m^2 - 1\ ,\\
E &= -\alpha_{23}u(u-1)U_p/8U_m^2\ ,\\
F &= [4U_mV_p+(uv+w+2I_2PQR)U_p]/U_p^2V_p\ ,
\end{aligned} \tag{A4}$$

where $U_p=1+u+2I_1PQ$, $V_p=v+I_1PR$, $U_m=U+I_2PQ^2$, and $F=(\rho_{123}+\rho_{312})n_I$. The parameters $I_j=[n_u\phi_u^j]_u/n_u\phi_u^j$ result from factoring $n_I\,\alpha'_{22}\,\phi_I$ out of the expresssions for the magnetoresistance. For example, recalling that τ_{ij} is dimensionless, we have

$$\sigma_{11}=\tfrac{1}{2}[n_I\phi_I]_I(\alpha'_{11}+\alpha'_{22})+[n_u\phi_u]_u\delta_1\tau_{11}^u$$

$$= n_l \phi_l \alpha'_{22} \left\{ \frac{(1+u)}{2} + \frac{n_u [n_u \phi_u]_u \phi_u \delta_1 \tau_{11}^u}{n_l n_u \phi_u \phi_l \alpha'_{22}} \right\}$$

$$= n_l \phi_l \alpha'_{22} [\tfrac{1}{2}(1+u) + P I_1 Q] \,. \tag{A5}$$

Here $P = n_u/n_l$ and can be evaluated from dHvA data, whereas $Q = \phi_u \delta_1 \tau_{11}^u / \phi_l \alpha'_{22}$ is effectively the ratio of the subscript 11 component of the upper-band mobility to the subscript 22 component of the lower-band mobility. For a highly degenerate sample, $[n\phi^j] = n\phi^j$ so that $I_j = 1$, but at 77 K, where the condition $E_F \gg k_B T$ is not satisfied, the parameters I_j are numerically evaluated assuming $\phi(E) = bE^{-1/2}$. If these correction factors are not used, instead of two parameters Q and R $(= \phi_u \delta_3 \tau_{33}^u / \phi_l \alpha'_{22})$, it would be necessary to include in the fit

$$[n_u \phi_u]_u \delta_1 \tau_{11}/n_l \alpha'_{22} \phi_l \,, \quad [n_u \phi_u^2]_u (\delta_1 \tau_{11}^u)^2/n_l \alpha_{22}^2 \phi_l^2 \,,$$

$$[n_u \phi_u^3]_u (\delta_1 \tau_{11}^u)^3/n_l \alpha_{22}^2 \phi_l^3 \,,$$

and three similar terms using $\tau_{33}^u \delta_3$. In our case, since we have only six experimental ratios, such a fit would not have been possible. Moreover, by eliminating the predictable effects of changing degeneracy, the parameters Q and R will reflect more accurately changes in the scattering time or band parameters.

For the single-band model [Eq. (A1)], there is an exact solution for the parameters A, B, C, and D in terms of u, v, w, and β. The result is quadratic in u, viz.,

$$a_1 u^2 + a_2 u + a_3 = 0 \,, \tag{A6}$$

where

$$a_1 = \frac{6}{A} - \frac{2}{C} \,,$$

$$a_2 = \frac{8-20A}{B} - \frac{4A}{C} + \frac{8A^2}{C(1+D)} \,, \tag{A7}$$

$$a_3 = \frac{4A+2}{B} - \frac{12A}{C} + \frac{2}{C} + \frac{8A^2}{C(D+1)} \,.$$

Using the above solution for u, v may be evaluated from

$$v = 16\beta u B/[(1-5u)(4A-1) + (3+u)] \,. \tag{A8}$$

Finally, w may be evaluated by substituting the solutions for v and u in the expression for A, and β may be evaluated using the value of u in the expression for D. Although an exact solution such as presented here is extremely useful for a rapid determination of u, v, w, and β from experimental data, the optimization procedure outlined in the text has the merit of including all the experimental data, as well as allowing for variable weighting to take account of experimental uncertainties.

To obtain the ratios $\tau_{11}\alpha_1/\tau_{22}\alpha_2$, etc., it is necessary to invert Eq. (9). The proper transformation is

$$\frac{\gamma_2}{\gamma_1} = \frac{c^2}{u} + \frac{s^2 v}{u} + 2sc(v-w)^{1/2} u \,,$$

$$\frac{\gamma_3}{\gamma_1} = \frac{s^2}{u} + \frac{c^2 v}{u} - \frac{2sc(v-w)^{1/2}}{u} \,, \tag{A9}$$

$$\frac{\gamma_4}{\gamma_1} = \frac{-sc(1-v)}{u} + \frac{(c^2-s^2)(v-w)^{1/2}}{u} \,,$$

where $s = \sin\theta$ and $c = \cos\theta$, θ being defined in Eq. (9).

---

†Work supported by the National Science Foundation. This paper is based on a thesis sibmitted by one of us (H. A.) as partial fulfillment of the requirements for the Ph. D. degree in Physics at Carnegie-Mellon University, Pittsburg, Pa. (unpublished).

*Present address: Department of Physics, Seton Hall University, South Orange, N. J.

[1]J. R. Drabble, R. D. Groves, and R. Wolfe, Proc. Phys. Soc. (London) 71, 430 (1958).

[2]J. R. Drabble, Proc. Phys. Soc. (London) 72, 380 (1958).

[3]J. R. Drabble, in *Progress in Semiconductors*, edited by A. F. Gibson and R. E. Burgess (Wiley, New York, 1963), Vol. 7, p. 45.

[4]R. B. Mallinson, J. A. Rayne, and R. W. Ure, Jr., Phys. Rev. 175, 1049 (1968).

[5]G. E. Shoemake, J. A. Rayne, and R. W. Ure, Jr., Phys. Rev. 185, 1046 (1969).

[6]B. Yates, J. Electron. Con. 6, 26 (1959).

[7]P. A. Walker, Proc. Phys. Soc. (London) 76, 113 (1960).

[8]R. W. Ure, Jr., in *Proceedings of the International Conference on Physics of Semiconductors, Exeter* (The Institute of Physics and The Physical Society, London, 1962), p. 659.

[9]B. A. Efimova, I. Ya. Korenblit, V. I. Novikov, A. G. Ostroumov, Fiz. Tverd. Tela 3, 2746 (1961) [Soviet Phys. Solid State 3, 2004 (1962)].

[10]L. R. Testardi, P. J. Stiles, and E. Burstein, Solid State Commun. 1, 28 (1963).

[11]I. A. Smirnov, E. V. Shadrich, and V. A. Kutasov, Fiz. Tverd. Tela 11, 3311 (1969) [Soviet Phys. Solid State 11, 2681 (1970)].

[12]R. V. Parfen'ev (private communication).

[13]P. M. Lee and L. Pincherle, Proc. Phys. Soc. (London) 81, 461 (1963).

[14]F. Borghese and E. Donato, Nuovo Cimento 53B, 283 (1968).

[15]S. I. Katsuki, J. Phys. Soc. Japan 26, 58 (1969).

[16]A. C. Smith, J. F. Janak, and R. B. Adler, *Electronic Conduction in Solids* (McGraw-Hill, New York, 1967), pp. 192 and 246; note that this text interchanges binary and bisectrix axes.

[17]J. R. Drabble and R. Wolfe, Proc. Phys. Soc. (London) 69B, 1101 (1956).

[18]C. Herring, Bell System Tech. J. 39, 237 (1955).

[19]C. Herring and E. Vogt, Phys. Rev. 101, 944 (1956).

[20]I. Ya. Korenblit, Fiz. Tverd. Tela 2, 3083 (1960)

[Soviet Phys. Solid State 2, 2738 (1961)].

[21]H. J. Mackey and J. R. Sybert, Phys. Rev. 172, 603 (1968).

[22]H. J. Mackey and J. R. Sybert, Phys. Rev. 180, 678 (1969).

[23]T. D. Fuchser, H. J. Mackey, and J. R. Sybert, Bull. Am. Phys. Soc. 15, 266 (1970).

[24]H. J. Goldsmid, J. Appl. Phys. 32, 2198 (1961).

[25]L. P. Caywood, Jr., and G. R. Miller, Phys. Rev. Letters 21, 1002 (1968); Phys. Rev. B 2, 2309 (1970).

[26]T. O. Yep and W. M. Becker, Phys. Rev. 144, 941 (1966).

[27]B. L. Booth and A. W. Ewald, Phys. Rev. Letters 18, 491 (1967).

[28]J. E. Robinson and S. Rodriguez, Phys. Rev. 135, A779 (1964).

[29]R. Hartman, Phys. Rev. 181, 1070 (1969).

[30]J. O. Jenkins, J. A. Rayne, and R. W. Ure, Jr., Phys. Letters 30A, 349 (1969).